IAEA nuclear fusion

PAPER • OPEN ACCESS

Multi-staged ERO2.0 simulation of material erosion and deposition in recessed mirror assemblies in JET and ITER

To cite this article: S. Rode *et al* 2024 *Nucl. Fusion* **64** 086032

View the article online for updates and enhancements.

You may also like

- Progress in research and development of mirrors for ITER diagnostics
A. Litnovsky, V. Voitsenya, T. Sugie et al.
- First mirrors for diagnostic systems of ITER
A. Litnovsky, V.S. Voitsenya, A. Costley et al.
- First mirror erosion–deposition studies in JET using an ITER-like mirror test assembly
M. Rubel, Sunwoo Moon, P. Petersson et al.

This content was downloaded from IP address 134.94.123.71 on 29/06/2026 at 07:22

OPEN ACCESS
IOP Publishing | International Atomic Energy Agency
Nuclear Fusion
Nucl. Fusion **64** (2024) 086032 (15pp)
https://doi.org/10.1088/1741-4326/ad556d

Multi-staged ERO2.0 simulation of material erosion and deposition in recessed mirror assemblies in JET and ITER

S. Rode[1,2,*], **S. Brezinsek**[1,2], **M. Groth**[3], **A. Kirschner**[1], **D. Matveev**[1], **L. Moser**[4], **R.A. Pitts**[4], **J. Romazanov**[1,5], **A. Terra**[1], **T. Wauters**[4] and **S. Wiesen**[1]

[1] Forschungszentrum Jülich GmbH, Institut für Energie- und Klimaforschung—Plasmaphysik, Partner of the Trilateral Euregio Cluster (TEC), 52425 Jülich, Germany
[2] Faculty of Mathematics and Natural Sciences, Heinrich Heine University Düsseldorf, 40225 Düsseldorf, Germany
[3] Aalto University, Espoo, Finland
[4] ITER Organization, Route de Vinon sur Verdon, Saint Paul Lez Durance, France
[5] JARA-HPC, Jülich Supercomputing Centre, Forschungszentrum Jülich GmbH, 52425 Jülich, Germany

E-mail: se.rode@fz-juelich.de

Received 16 January 2024, revised 28 May 2024
Accepted for publication 7 June 2024
Published 25 June 2024

Abstract
The deposition/erosion on optical diagnostic components—mirrors—is a critical issue in reactor class devices with long-pulsed high fluence plasma operation. The paper presents results of the three-dimensional Monte–Carlo code ERO2.0 for two diagnostic aperture and first mirror geometries to be deployed in ITER, along with a separate simulation study that aims to replicate results from an experimental first-mirror study carried out on JET. Promisingly, very little plasma and impurity deposition on mirrors for the anticipated plasma durations is found in the ERO2.0 modelling taking into account the current ITER Research Plan and a material mix with beryllium first wall and a tungsten divertor. The post-mortem analysis of mirrors exposed during the experiment and the initial benchmarking efforts on the JET mirror experiment are also broadly consistent, increasing the confidence in predictions for ITER.

Keywords: ERO2.0 code, erosion, first mirror, ITER, JET, diagnostic first wall

(Some figures may appear in colour only in the online journal)

[*] Author to whom any correspondence should be addressed.

Original Content from this work may be used under the terms of the Creative Commons Attribution 4.0 licence. Any further distribution of this work must maintain attribution to the author(s) and the title of the work, journal citation and DOI.

© 2024 The Author(s). Published by IOP Publishing Ltd on behalf of the IAEA

1. Introduction

Mirrors are used in many in-vessel optical diagnostic systems in fusion devices like JET and will be employed in ITER. To avoid extensive erosion and deposition from plasma fuel ions, charge-exchange neutrals (CXN) or impurity particles from gas seeding or main wall sputtering, the mirrors are in general placed far away from the main plasma, with apertures designed small to avoid high loads onto the mirrors and to act as an optimised neutron shield. Nevertheless, a small fraction of particles will either directly impact the first mirrors (FMs) by line-of-sight transport through apertures or erode material from the aperture surfaces, which can subsequently reach mirror surfaces, leading to erosion and deposition of the surface. Both erosion and deposition can impact the performance of the optical diagnostic, as specular reflection and the reflection homogeneity is reduced, which negatively affects imaging diagnostics. Thus, a thorough analysis of the expected incoming particle fluxes, their energy distributions and their interactions with the surfaces is required to determine their potential impact on the mirror material. An analysis has been conducted before [1], but did not consider re-erosion and deposition of impurities along the tunnel to the mirror and was not performed in full 3D, leading to large uncertainties in the results. These aspects are crucial to assess the operational lifetime of the optical diagnostics, corresponding to the order of 10^7 s of plasma time in more than ten years of expected ITER operation.

The Monte–Carlo code ERO2.0 [2] can provide local erosion and deposition fluxes at plasma-facing components in full 3D. However, in far recessed areas like mirror assemblies, the code is approaching its limits due to low statistics, as typically only one in more than 10^8 simulated particles from the main plasma reaches the mirror's location [3]. A reasonably high number of particles at the key components is necessary to allow collection of representative energy and angular distributions for erosion and deposition predictions. In far recessed areas, this resolution cannot be achieved with standard simulations.

A novel multi-staged approach based on ERO2.0 simulations was developed and introduced in [3] to overcome this challenge (see figure 1 for a simplified overview of the workflow). The simulation chain from the main plasma to the mirror location is split into three stages for each mirror assembly—global, intermediate and final. Particles from each simulation stage are collected at virtual surfaces (called 'catcher planes'), which serve as interfaces between the simulation stages. The collection of particle statistics, e.g. energy and impact angle, at the interface allows sampling a large number of particles which are injected into the next simulation stage and represent the original fluxes, spread over the catcher plane. The statistics in far recessed regions is drastically increased by this multiplication of the amount of simulated test particles. The desired quality of results in remote areas can thus be reached with this approach, providing important predictions for the operation of optical diagnostics. For a more detailed explanation of the multi-stage simulation setup, please refer to [3].

The four main codes used for the ITER and JET simulation setup in this work are:

- SOLPS-4.3 [4] (a multi-fluid plasma transport code including the plasma code B2 and EIRENE), providing the plasma boundary solutions for ITER. The simulated plasma volume is extended to the apex of the first wall with OEDGE [5] via onion-skin modelling and EIRENE;
- EDGE2D-EIRENE (including the 2D fluid edge code EDGE2D and EIRENE), providing the JET plasma solutions;
- EIRENE [6], a 3D neutral particle transport code, used inside OEDGE, SOLPS-4.3 and EDGE2D-EIRENE, but also used for sampling incoming deuterium neutral particle fluxes onto the mirror assemblies;
- ERO2.0 [2], a 3D Monte–Carlo code using the provided plasma simulations to trace impurities throughout the plasma edge to estimate local erosion and deposition fluxes at plasma-facing components. A database of SDTrimSP [7] simulations (a surface sputtering code using binary-collision approximation) is used for the plasma-wall interaction.

In this paper, only results for the final stages (conducted purely in ERO2.0) of each simulation are shown, focussing on the results on the mirror surfaces themselves. Three geometries are presented: two FMs planned in the Equatorial and Upper Port of the ITER Diagnostic First Wall (DFW) exposed in three different plasma cases representing the whole ITER lifetime; and a mirror assembly in the JET outer mid-plane that was exposed in a mix of H-mode and L-mode plasmas. The JET case corresponds to an experiment conducted in the device in the third JET campaign with ITER-like wall consisting of beryllium (Be) main chamber and tungsten (W) divertor. The mirrors were thoroughly analysed post-mortem in [8], so a comparison of the simulation results to this experiment is conducted.

2. Plasma cases, geometry and charge-exchange spectra

2.1. ITER

For ITER, a Be first wall and a W divertor were assumed, of which only the first wall was considered as source for sputtered material, since the transport from the divertor up to the relevant areas in the main chamber is negligible. The first stage of the simulation setup was conducted in a 20° sector of ITER with periodic boundary conditions. In the further stages, models for the DFW (iron, Fe), first and second mirrors (molybdenum, Mo) and their respective holders (Fe) were included—an overview of the mirror assemblies can be seen in figure 2 with locations of the ports in the global simulation volume designated. It should be noted that pure iron was used as a proxy for the ITER steel, as it has the highest concentration and lowest sputtering threshold of the materials used in the steel. The materials can mix in a 100 nm surface interaction layer, for which a homogeneous mixing model (HMM) is used in ERO2.0, allowing

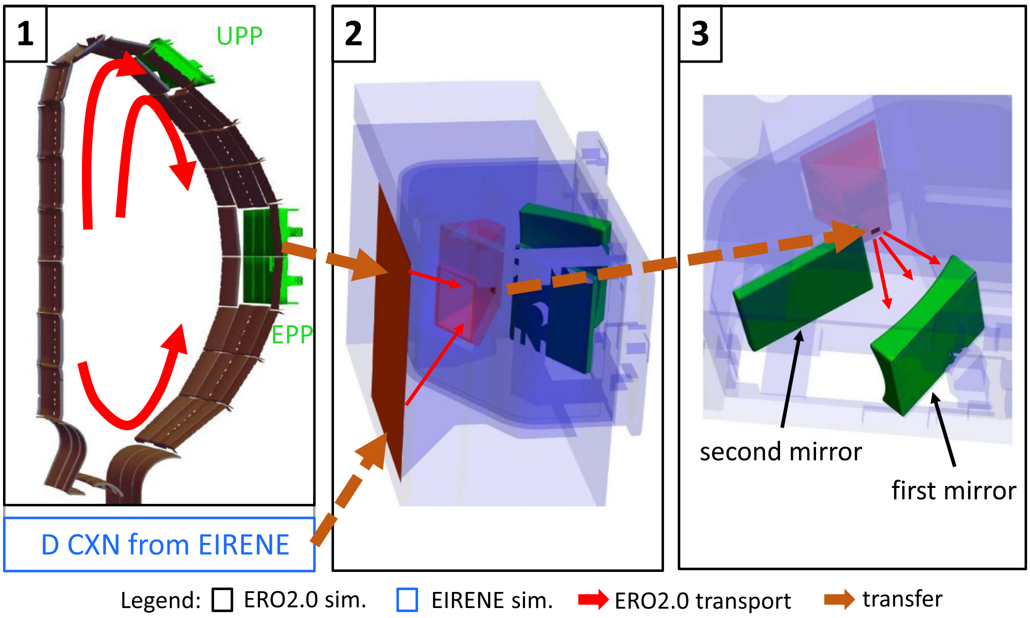

Figure 1. Simplified overview of the three-stage simulation setup used for all JET and ITER simulations in this work, shown here for the ITER equatorial port plug (EPP). Stage 1: global modelling with diagnostic surfaces covering the entrance to recessed area (here: DFW in equatorial (EPP) or upper port plug (UPP)). Stage 2: local modelling covering entrance of DFW labyrinth. Stage 3: local modelling from aperture hole to mirror volume. For a detailed explanation of the workflow, see [3] on which this graphics is also based on. Reproduced from [3]. CC BY 4.0.

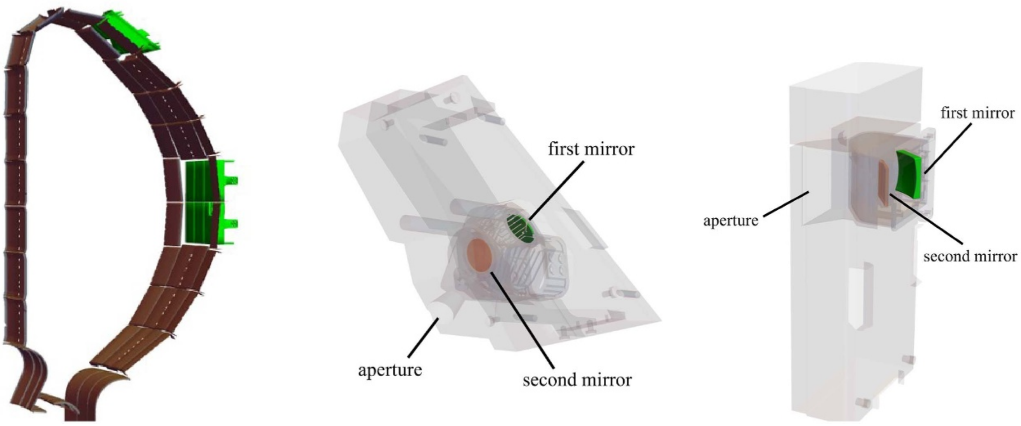

Figure 2. Geometry used for the ITER mirror simulations. Left: global 20° simulation volume of ITER with positions of upper and equatorial port DFWs in green, Be first wall and W divertor. Middle and right: local simulation volumes in the upper port (middle, seen from the plasma side) and equatorial port (right, seen from the rear side) with diagnostic first wall in grey, first mirror in green and second mirror in orange.

surface concentration changes over the discretised simulation time.

Three plasma cases were analysed in this work: two H-mode cases corresponding to deuterium-fuelled fusion-power operation (FPO) and one L-mode case from pre-fusion-power operation (PFPO) with H fuel (see table 1). The 2D plasma background for each case (provided by OEDGE through the ITER organisation) is assumed to be toroidally symmetric throughout the 3D ERO2.0 simulation volume, which consists of a 20° sector of ITER with periodic boundary conditions in toroidal direction. Values in the region of the mirror assembly far outside the main plasma and behind the first wall were extrapolated, as no plasma code extends up to this region. With a decay length of 1 cm used, the values inside the assembly essentially correspond to vacuum (e.g. for case #1: $T_e \sim 10^{-5}$ eV, $n_e \sim 10^{12}$ m^{-3}) in both ports (see [9] for a sensitivity study including extrapolation profiles). The plasma codes also provide information about the plasma fuel fluxes onto the first wall and divertor—these ion fluxes are used in the global (first) stage of the simulation and contribute to sputtering. The recessed areas are assumed to be plasma-shadowed areas, so sputtering by the plasma background is not performed in the intermediate stages of the approach.

Inside the plasma volume, particles are subject to the Lorentz force, collisions with the charged plasma background

Table 1. Definition of ITER plasma cases for ERO2.0 simulations in this work. P_{SOL} is the power flowing to the scrape-off layer (SOL). See [10] for more information on the SOLPS-4.3 plasma modelling.

Label in this work	Label in [10]	Density	Fuel	sim. time (s)	Comments
Case #1	Case #1	High	D	$8 \cdot 10^6$	Baseline $Q = 10$ H-mode burning plasma (nominal 15 MA, 5.3 T, $P_{SOL} =$ 100 MW), high far-SOL density, zero imposed SOL flow.
Case #2	Case #3	Low	D	$8 \cdot 10^6$	Baseline $Q = 10$ H-mode burning plasma (nominal 15 MA, 5.3 T, $P_{SOL} =$ 100 MW), low far-SOL density, zero imposed SOL flow.
Case #3	Case #7	Low	H	$9 \cdot 10^5$	Baseline hydrogen L-mode, characteristic of basic divertor operation in low power, non-active phases (nominal 7.5 MA, 2.65 T, $P_{SOL} = 20$ MW), low far-SOL density, zero imposed flow.

(treated via a Fokker–Planck equation) and neutral background particles (treated as hard sphere collision), as well as potentially ionisation and recombination. Anomalous diffusion is assumed only in the global stage with a diffusion constant of 1.0 m^2/2, and disabled in the later stages, where most traced particles are neutral anyway. Electric fields outside of the sheath region and thermal force effects are not considered in this work, because the simulations are based on older plasma backgrounds which do not include information about these effects.

Global ITER first wall modelling using ERO2.0 has been conducted for these plasma cases in the past ([10], see table 1 for corresponding case numbers), but no analysis of the recessed regions has been performed prior to this work for these plasmas.

2.2. JET

For JET, a mirror assembly using an ITER-like arrangement is the focus of the simulation. The nickel (Ni, used here as a proxy for Inconel used in JET) mirror assembly considered in this paper has three entrances, two of which (A and B) have a cone-like structure in front of them. All three entrances lead to one closed volume inside the assembly where three Mo mirror locations are positioned. The geometry and an overview of the position of the assembly in the JET outer mid-plane can be seen in figure 3. It should be noted that the geometries used as mirrors here correspond to the mirror holders, because no models for the mirrors themselves were available. In the experiment, two mirrors were placed on each mirror holder. The simulation results on the mirror holders should however be nearly identical, because the actual mirror surfaces are parallel to the holders, although a slightly larger surface is considered. From this point on, the mirror holder geometries in JET will be simply referred to as mirrors.

Two plasma cases are considered for the JET modelling, one H-mode and one L-mode case, see table 2. For the plasma background data, existing EDGE2D-EIRENE solutions for L-mode and low-power H-mode at 2.0 MA, 2 T in semi-horizontal configuration—so-called V5 - based on earlier studies were used [11]. The H-mode plasma is close to the average H-mode in the phase of operation. In the plasma modelling, EDGE2D-EIRENE assumes a profile for anomalous diffusion coefficient (see [12]) with values close to 1.0 $m^2 s^{-1}$ throughout the whole volume. ERO2.0 uses a constant value of 1.0 $m^2 s^{-1}$ for simplicity.

All plasma parameters provided by EDGE2D-EIRENE as 2D maps were considered toroidally symmetric throughout the ERO2.0 simulation volume in the first stage of the simulation. The simulation volume includes the full 360° model of JET, as due to the irregular pattern of the poloidal limiters in JET, no periodic boundary conditions can be used in contrast to ITER. Plasma background parameters in the region of the mirror assembly were again extrapolated as in the previous section, although it should be noted that EDGE2D-EIRENE plasma solutions do not reach up to the apex of the wall as it was the case for ITER OEDGE solutions.

2.3. Energy spectra of CXNs

CXNs play a significant role in the simulation of erosion in recessed areas. Therefore, special emphasis was put on the simulation of the energy spectra of neutral fuel particles entering the relevant areas. These spectra were generated by EIRENE post-processing of the existing SOLPS-4.3 and EDGE2D-EIRENE simulations described in sections 2.1 and 2.2 (for a more detailed explanation of the process please refer to [3]). The spectra generated in this process can be seen in figure 4. Note that for all ITER cases, binning was performed in bins of 0.15 eV width up to 1500 eV, and in bins of 5 eV up to 2000 eV in the JET cases. For figure 4, the ITER data has been post-processed to a bin width of 5 eV for a better comparability between all cases.

3. Results

Before the analysis of the results, the following definitions are used in this paper:

- gross deposition [atoms cm^{-2}]: all particle fluxes impinging on a surface (not counting reflected particles), normalised by the surface area, integrated over simulation time;
- gross erosion [atoms cm^{-2}]: all particle fluxes eroded from a surface, normalised by surface area, integrated over simulation time;
- net fluence [atoms cm^{-2}]: gross deposition minus gross erosion on each surface cell—negative values show net

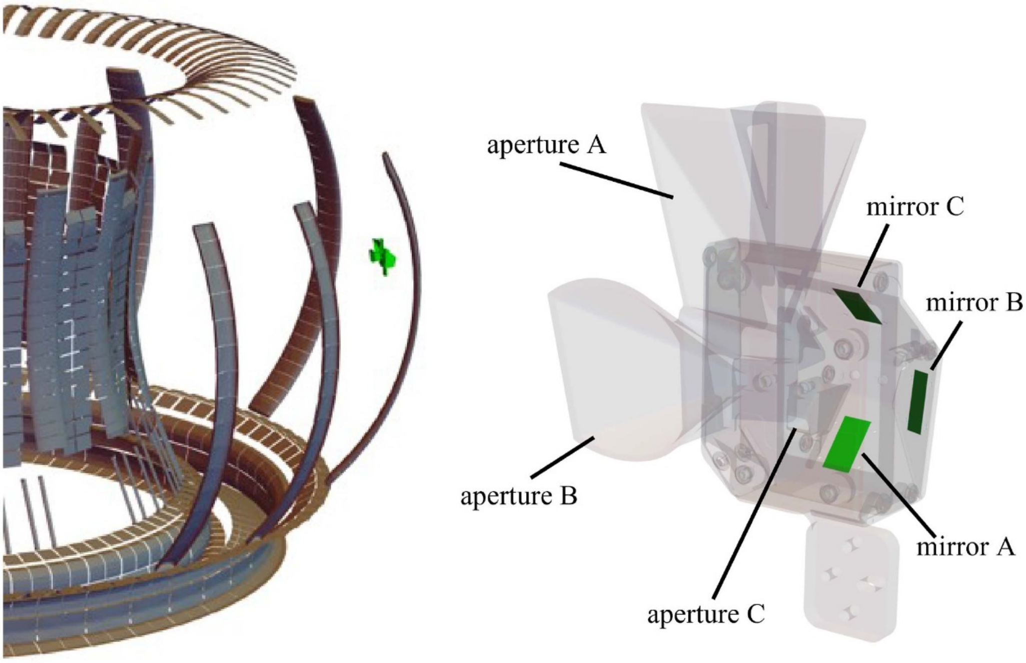

Figure 3. Geometry used for JET modelling—left: position of the mirror assembly (green) in the JET device (Be first wall and W divertor in grey—only half of the device is shown here, but the simulation includes the full 360° geometry). Right: local simulation volume with mirror assembly in grey and mirrors A, B and C in green. The apertures leading to mirrors A and B are equipped with an entrance cone, respectively.

erosion, positive values show net deposition zones. Scales with the exposition time of each case;

- layer growth (nm) (... rate [nm s^{-1}]): an estimate of the eroded/deposited thickness, generated by converting the particle fluxes to volumetric fluxes using the element's density;
- concentration: ERO2.0 uses a HMM for surface composition changes in the volume defined by the surface area of each geometry polygon and a set surface interaction layer thickness d (input parameter). The concentrations shown in the following sections are thus the 'surface concentration' within the surface interaction layer of thickness d, i.e. the volume concentration in this interaction volume;
- surface interaction layer thickness d: the net fluxes in each time step of ERO2.0 are converted to a volume flux and this volume (i.e. the impinging particles) is assumed to redistribute homogeneously in a surface interaction layer of thickness d, which is an input parameter. Higher values mean proportionally slower concentration changes because a larger volume is mixed. Re-erosion is only possible from the surface interaction layer in ERO2.0. Importantly, the choice of d does not influence steady-state results but is only relevant here because a defined physical simulation time (corresponding to the experimental exposure time (JET)/ the FPO or PFPO phase time (ITER)) was set. Furthermore, the computed fluences [atoms m^{-2}] are only in second order dependent on the surface interaction layer thickness via the re-erosion of the interaction volume—in deposition dominated regions, as the FMs are, the re-erosion is nearly negligible so the net fluence should be largely independent of d.

Table 2. Definition of JET plasma cases for ERO2.0 simulations in this work. See [12] for more information on the EDGE2D-EIRENE plasma modelling.

plasma case	$n_{e,sep,omp}$ $(/m^3)$	$P_{core,E2D}$ (MW)	Fuel	sim. time (s)
H-mode	$3.0 \cdot 10^{19}$	4.8	D	$3 \cdot 10^4$
L-mode	$1.4 \cdot 10^{19}$	2.2	D	$5.5 \cdot 10^4$

3.1. Results for ITER case #1: high density H-mode

From the three analysed plasma cases in ITER, case #1 shows the highest erosion and deposition fluxes onto the FM. For this reason, case #1 is shown here in detail, while an overview of the other two plasma cases can be found in section 3.2. For this case, a total simulation time of 8×10^{-6} s (∼2200 h) was assumed, corresponding to the total planned plasma time of all three active (FPO) ITER campaigns [13]. It should be noted that the provided high-power plasma background was assumed constant throughout the whole simulation time, thus no limiter phase or other low power H-mode discharges are included in the modelling.

As an additional note, the analysis focusses on the FM in each port—the second mirrors in both the equatorial and upper port (orange in figure 2) are in general reached by about 10% of the fluxes impinging on the respective FM, in addition to some Mo sputtered from the FM. Due to additional reflections before reaching the second mirror, the impinging energies are lower and thus all elements are net deposited, but due to the far lower fluxes, even thinner deposits are found here, which is why no figures for second mirrors are shown in this work.

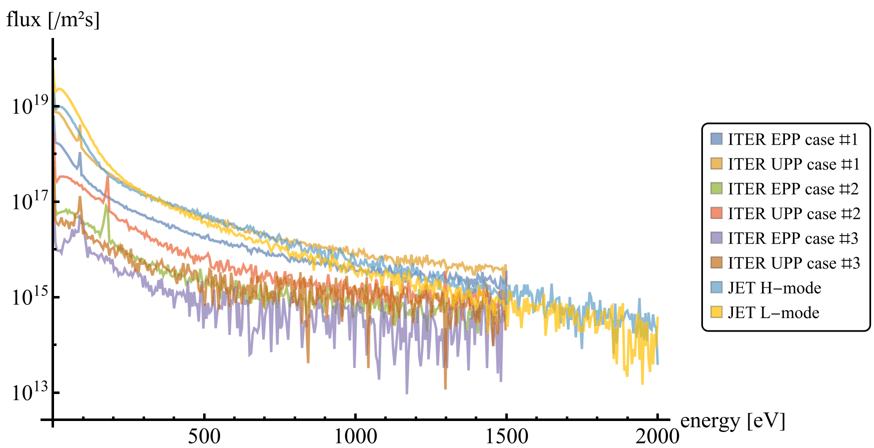

Figure 4. Energy spectra of neutral fuel particles entering the recessed region of the mirror assemblies (JET) and DFW (ITER) generated by EIRENE. See tables 1 and 2 for details about the plasma backgrounds.

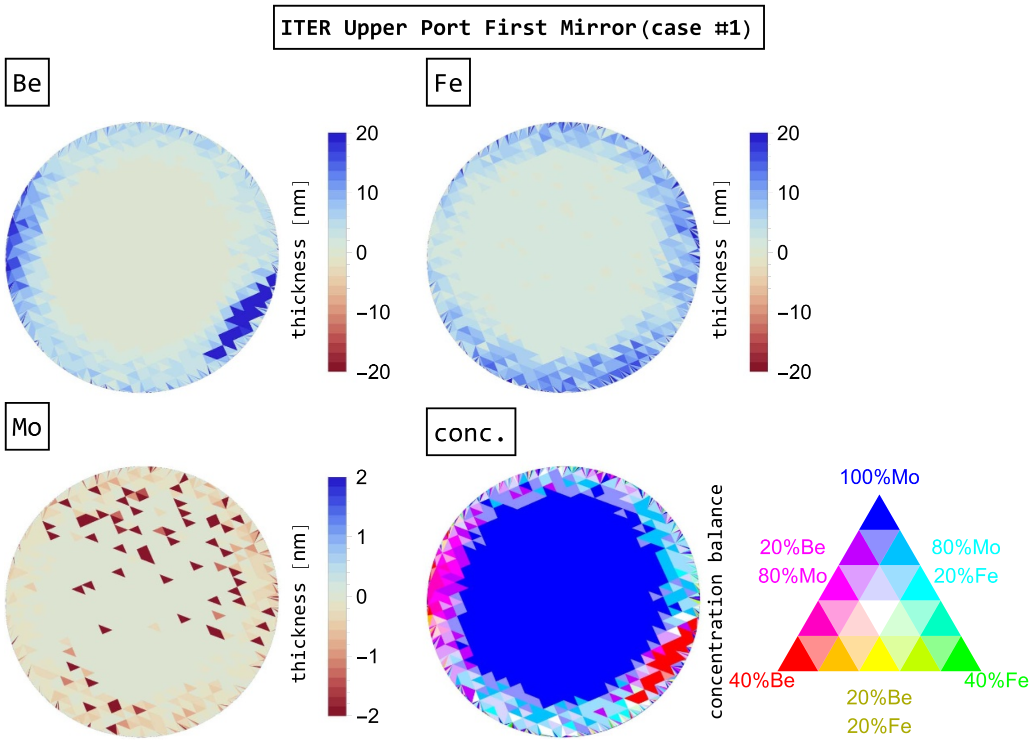

Figure 5. Net fluence of Be (top left), Fe (top right) and Mo (bottom left) on the upper port first mirror—net erosion is shown in red, net deposition in blue. Bottom right picture shows surface composition in a 100 nm surface layer.

An overview table of average deposition values on both first and second mirrors in all simulated plasma cases can be found in section 3.2.

3.1.1. Results for the ITER upper port FM. Figures 5(*a*)–(*c*) shows the FM's front surface. The accumulated Be, Fe and Mo net fluences at the end of the simulation time are depicted—Be (originating from the main chamber) and Fe (sputtered from the DFW itself) are deposited (depicted in blue), while Mo (the mirror material) is net sputtered. Some Mo is also deposited on the FM, originating from sputtering of the second mirror (orange in figure 2, the second mirror is not shown here further), which is included in the net fluences depicted on the FM. Figure 5(*d*) shows the surface composition in a surface interaction layer thickness $d = 100$ nm, all polygons of the mirror stay above 60% Mo. No steady state concentrations were reached, because the fluxes into the remote areas are so small, which means that the concentration value (as explained above) after the fixed simulation time depends on the choice of d via the size of the interaction volume. Recently performed SDTrimSP studies suggest interaction layers of less than 5 nm thickness for the typical projectile velocities which is lower than the 100 nm assumed in the ERO2.0 simulations. A smaller d would lead to more re-erosion of the impurities on the surface, so the shown fluences should be seen as an upper

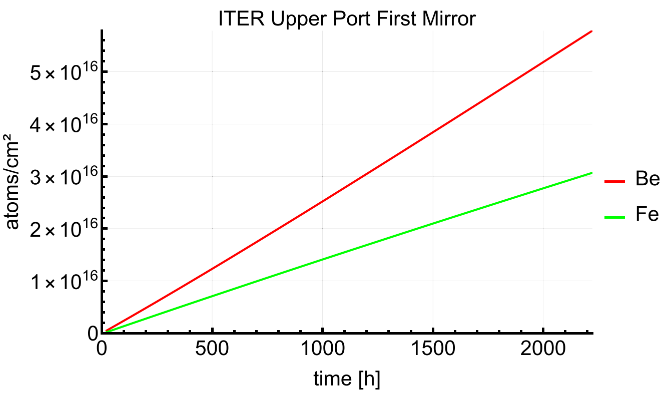

Figure 6. Net fluences of Be and Fe on front of the upper port first mirror surface over the ITER FPO time, averaged over the mirror front surface. The surface simulation was performed in 100 equidistant time steps.

bound, while the surface impurity concentrations can be seen as a lower bound.

Overall, a strong geometrical pattern was observed, for which the edge of the mirror shows much higher fluence and the mirror centre is nearly unaffected—the net values for Fe/Be deposition and Mo erosion lie well below 1 nm (corresponding to barely a mono-layer) in the central part, while values at the edge are on the order of few nm deposition. This pattern is directly attributed to the geometry of the mirror assembly right in front of the mirror: a cone-like structure (lower left part in figure 2) leads from the plasma side to the mirror volume. Because of the low temperatures inside the volume and recombination at the PFCs, most particles recombine and stay neutral throughout the simulation in the mirror assembly. Background neutral atomic densities are low enough to barely affect the transport, so the transport of these particles is mostly ballistic. This means that particles reflected or sputtered from the cone structure 'see' only a part of the mirror, which is exactly the edge of the mirror and thus explains the preferential deposition in this region.

In figure 5(*c*), one further notices single cells (dark red triangles) signifying very strong Mo erosion values. These values lie far outside the shown colour scale in the range of 5–40 nm and can be attributed to single D CXN particles that passed all simulation stages without a collision. These particles have a high energy and represent a large number of real fluxes, leading to a very high sputtering yield. Even with the three-stage approach used here, the resolution is not good enough to resolve these rare particles in sufficient quality. However, since these 'unperturbed' particles in reality likely spread evenly over the mirror, and most sputtering is caused by D particles (see table 3), the area-averaged Mo erosion value over the mirror front surface (1.30 nm) is a more realistic interpretation of the result for the FM.

Over the entire simulation time, the net fluence of impurities on the FM increases almost linearly (see figure 6), as the surface processes are deposition-dominated and re-erosion does not play a big role. This can specifically be seen in table 3, where the erosion values of Fe and Be on the mirror are around one order of magnitude lower than the respective deposition. The highest fluence onto the mirror comes from D, which contributes to sputtering but D deposition or implantation is not tracked in the ERO2.0 code. Thus the net fluence is set to zero and D does not play a part in the concentration changes of the surface.

Concerning deposition, Be is the most significant element, with Fe fluxes being around 50% lower. Some Mo is also deposited on the mirror, originating from sputtering of the second mirror. Nearly all material on the mirror is sputtered by incoming D, caused by the comparatively high fluence coupled with the potentially high energy of the CXN particles. Be is the source of around 1.5% of the sputtering, while sputtering by Fe and Mo is negligible.

Finally, figure 7 shows the energy spectrum of the atoms impinging on the mirror split by element. Deuterium energies reach up to the highest energies due to the long high-energy tail of the incoming CXN spectrum, but because these particles mainly sputter Be and Fe inside the assembly, those elements can also be present at high energies—their mean energies are still far lower though.

3.1.2. Results for the ITER equatorial port FM. For the modelling of the transport in the equatorial port, the same parameters as for the upper port are applied, so the same approximations and caveats are valid (see section 3.1.1). Although the geometry in general and the shape of the mirrors are very different from the upper port, the results show the same general behaviour: Be and Fe are deposited in the order of up to 10 nm in the edge regions, while Mo is eroded (figure 8). The erosion shows strong outliers in the data of up to 20–70 nm erosion again due to statistics, but the area-averaged erosion value on the mirror front is 2.5 nm. Only the left rim of the mirror shows significant concentration changes, although the Mo concentration in the 100 nm interaction layer stays above 75% in nearly all cells. Sputtering is caused nearly exclusively by D and re-erosion is insignificant (table 4), but in the equatorial port, slightly more Fe than Be is deposited in total on the mirror (figure 9).

3.2. Overview of results for other ITER plasma backgrounds

The other two plasma cases from table 1 (case #2: low density H-mode and case #3: hydrogen L-mode) were simulated in the same way. The main findings are that in H-mode operation, more material is eroded and deposited than in the L-mode case, particularly in the high far-SOL density case #1 presented in detail in section 3.1. This is partially due to the longer operation time in H-mode (compare table 1), but also due to higher fluxes into the DFW ports. The general results show the same trends as the case #1 analysis: the deposition is much stronger on the edge regions of the mirrors, due to the 3D geometry of the cone leading up to it, but the magnitude of deposition and erosion strongly depends on the plasma case. Overall,

Table 3. Net surface fluences averaged over the front surface of the ITER upper port first mirror after integration over the ITER FPO time (second column). The other columns show the split between deposition and erosion, and the contribution of the different projectiles to the sputtering of each element. D is not deposited in the surface, but is assumed to recycle instantaneously. The front side of the mirror measures 201.7 cm^2.

ITER Upper Port First mirror	Net fluence [atoms cm^{-2}]	Gross deposition [atoms cm^{-2}]	Gross erosion [atoms cm^{-2}]	..by D %	..by Be %	..by Fe %	..by Mo %
D	0.00	2.79×10^{18}	0.00	—	—	—	—
Be	5.78×10^{16}	6.51×10^{16}	7.28×10^{15}	97.64	2.36	2.09×10^{-3}	4.7×10^{-6}
Fe	3.07×10^{16}	3.22×10^{16}	1.51×10^{15}	98.29	1.67	0.04	1.31×10^{-4}
Mo	-8.35×10^{15}	4.48×10^{13}	8.39×10^{15}	99.12	0.85	0.04	3.62×10^{-4}
total	8.02×10^{16}	2.88×10^{18}	1.72×10^{16}	98.42	1.56	0.02	1.9×10^{-4}

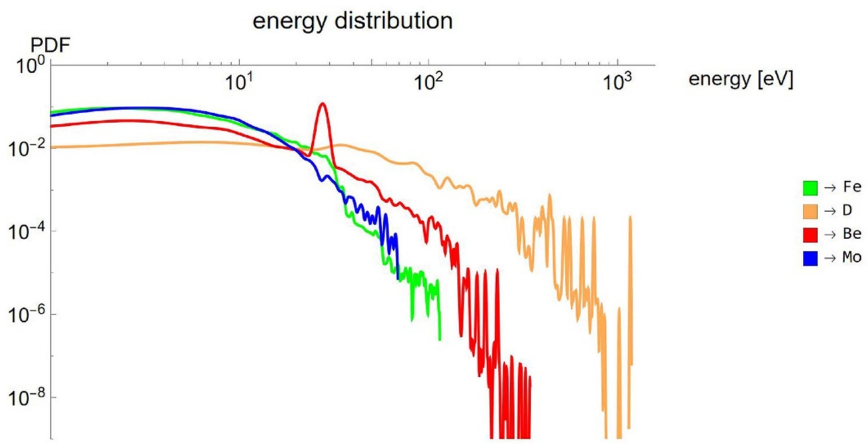

Figure 7. Energy spectrum of impinging particles on the upper port first mirror front surface by element for plasma case #1. The mean energies are D: 75 eV, Be: 20 eV, Fe: 9 eV, Mo: 9 eV.

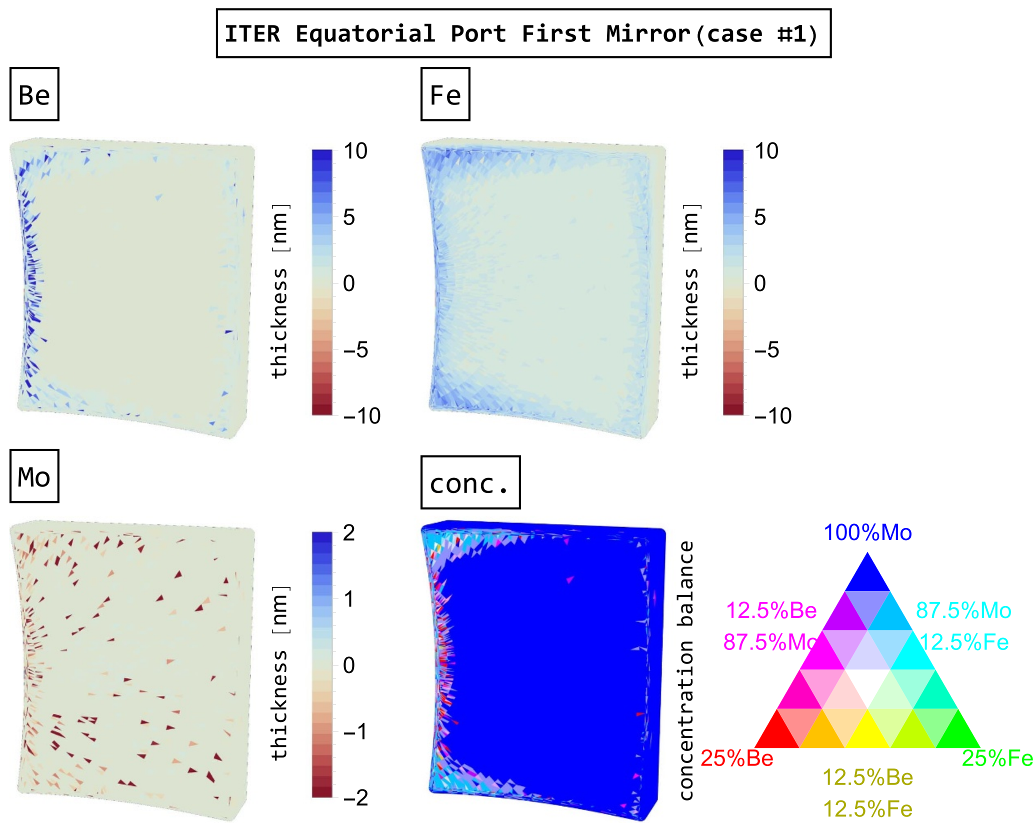

Figure 8. Net fluence of Be (top left), Fe (top right) and Mo (bottom left) on the equatorial port first mirror—net erosion is shown in red, net deposition in blue. Bottom right picture shows surface composition in a 100 nm surface layer.

Table 4. Net surface fluences averaged over the front surface of the ITER equatorial port first mirror after integration over the ITER FPO time (second column). The other columns show the split between deposition and erosion, and the contribution of the different projectiles to the sputtering of each element. D is not deposited in the surface, but is assumed to recycle instantaneously. The front side of the mirror measures 174.2 cm^2.

ITER Equatorial Port First Mirror	Net fluence [atoms cm^{-2}]	Gross deposition [atoms cm^{-2}]	Gross erosion [atoms cm^{-2}]	..by D %	..by Be %	..by Fe %	..by Mo %
D	0.00	1.89×10^{18}	0.00	—	—	—	—
Be	8.62×10^{15}	9.36×10^{15}	7.40×10^{14}	97.33	2.67	2.66×10^{-3}	3.12×10^{-4}
Fe	1.24×10^{16}	1.27×10^{16}	3.03×10^{14}	99.10	0.79	0.11	8.05×10^{-3}
Mo	-1.61×10^{16}	6.34×10^{14}	1.67×10^{16}	99.86	0.09	0.04	6.57×10^{-3}
total	4.92×10^{15}	1.92×10^{18}	1.77×10^{16}	99.74	0.21	0.04	6.33×10^{-3}

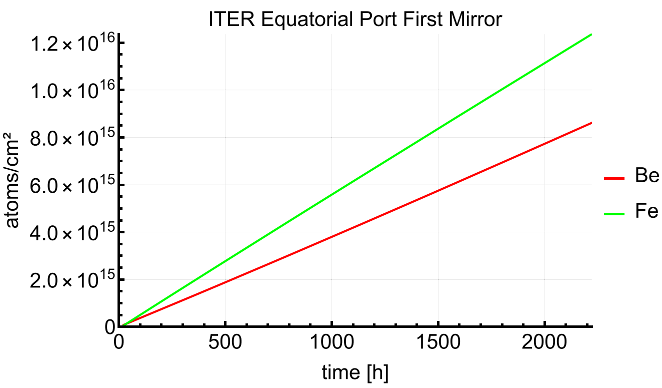

Figure 9. Net fluence of Be and Fe on front of the equatorial port first mirror surface over the ITER FPO time, averaged over the mirror front surface. The surface simulation was performed in 100 equidistant time steps.

Table 5. First mirrors: overview of average Mo erosion and Be and Fe deposition on the front of the mirror surfaces at the end of the simulation time—fluxes simulated by ERO2.0 were integrated over time and mirror front surface, and converted to a layer thickness using the element's density. Negative values imply net erosion.

		Mo layer (nm)	Be layer (nm)	Fe layer (nm)
case #1	Upper	−1.30	4.71	3.65
	Equatorial	−2.51	0.70	1.47
case #2	Upper	−0.23	1.29	0.30
	Equatorial	−0.19	0.07	0.19
case #3	Upper	-2.99×10^{-3}	0.02	3.27×10^{-3}
	Equatorial	-1.87×10^{-3}	1.03×10^{-3}	2.36×10^{-3}

only a few nanometers of molybdenum erosion are expected on average over the mirror front surfaces. Table 5 shows the area-averaged time-integrated values for the three elements in each simulation as an overview. Due to the strong geometrical dependency of the fluxes, the 3D pictures for the two mirrors in both plasma cases are shown in figures 10–13 (please note the scales which were chosen differently for each case due to strong differences in the magnitude). For the second mirrors, much less deposition is found, and the deposition is much more evenly spread out over the mirror front surface due to the additional reflections needed to reach the second mirror. An overview table for the deposition values on the second mirror can be found in table 6.

3.3. Results for JET and experimental comparison

For the JET setup, two simulations were performed (for plasma background details see table 2) with simulation times equal to the time in H-mode/L-mode discharges respectively that the mirrors were exposed to in the experiment in the ILW-3 campaign [8]. For the mirror assembly, a surface interaction layer thickness d of 100 nm was chosen. For the mirrors, d was set to 1 nm in this case. This value was chosen based on sample SDTrimSP simulations using energy and angle distributions found on the mirrors in preliminary simulations, so the concentration values on the mirror shown below should be as realistic as possible with the HMM used in ERO2.0. Because the three mirrors show very similar behaviour, only mirror A results are shown with 3D pictures in figures 14 and 15 respectively for the two plasma cases, while an overview of the deposition values and an experimental comparison can be seen in table 7.

The general results show the same trend as in the ITER cases: Be and Fe are deposited in small quantities (less than 1 nm everywhere on the mirror), with Ni values around one order of magnitude higher than for Be in the H-mode case (figure 14). Still, even for Fe, barely a monolayer is deposited on average on the mirror. Considering the erosion, the results show less statistical noise than in the ITER cases, which is likely caused by the much lower resolution of the geometry (256 cells for JET mirror A compared to around 4000 cells upper port FM front surface in ITER). As mentioned in section 2.2, the model only represents the mirror holder anyway, so more resolution is not meaningful. The area-averaged value of Mo erosion is 0.003 nm in H-mode. Concerning the concentrations, a rather homogeneous composition of around 85% Mo is reached, with Ni making up the largest fraction of the impurities. L-mode fluences are slightly higher and Ni concentrations of up to 50% can be found, which is partially due to the roughly twice as long exposure time in L-mode compared to H-mode. In contrast to the presented ITER cases, it is apparent that no geometrical pattern can be found—this is indeed not caused by the lower resolution, but instead because the cones leading to the mirrors (compare figure 3) are shaped in a way so that no particle starting/reflecting from the cone can directly see the mirror. Thus, no specific pattern is found on the mirror and the fluxes in general are very low, as nearly

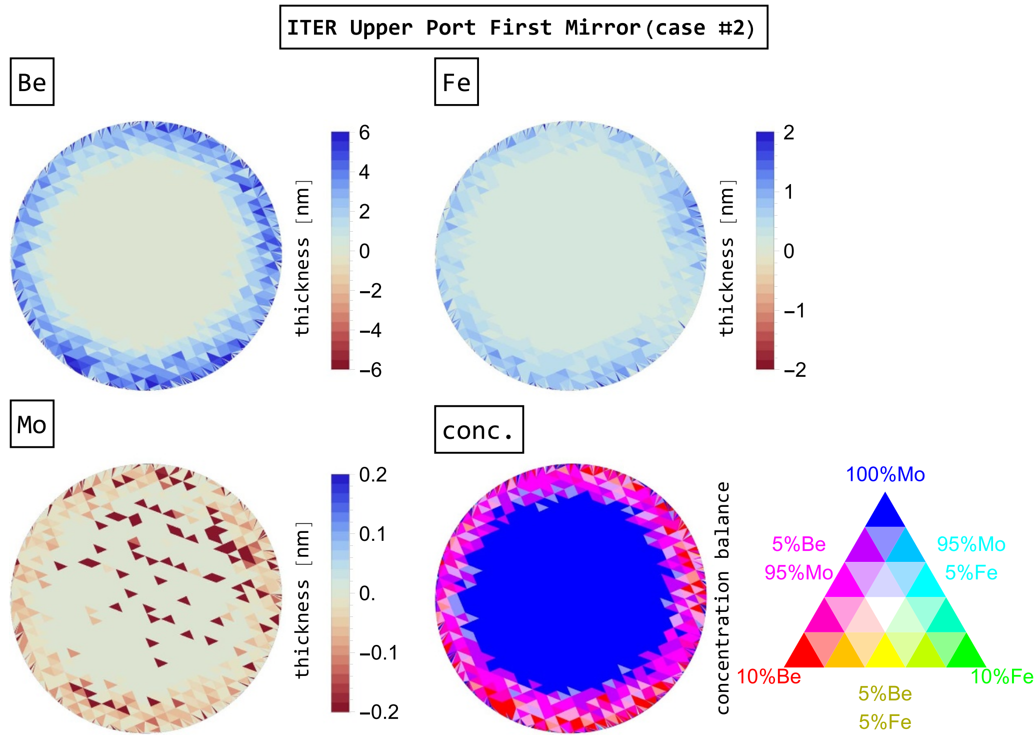

Figure 10. Net fluences of Be (top left), Fe (top right) and Mo (bottom left) on the upper port first mirror front surface at the end of the simulation—net erosion is shown in red, net deposition in blue. Bottom right picture shows surface composition in a 100 nm surface layer.

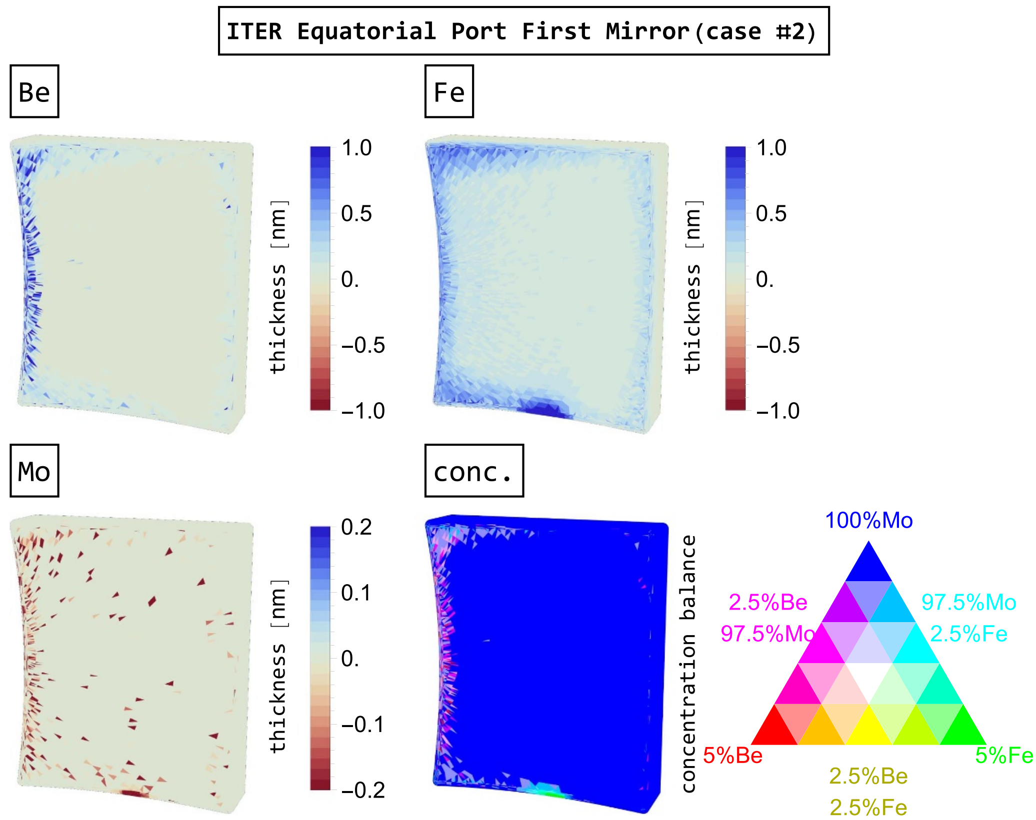

Figure 11. Net fluences of Be (top left), Fe (top right) and Mo (bottom left) on the equatorial port first mirror front surface at the end of the simulation—net erosion is shown in red, net deposition in blue. Bottom right picture shows surface composition in a 100 nm surface layer.

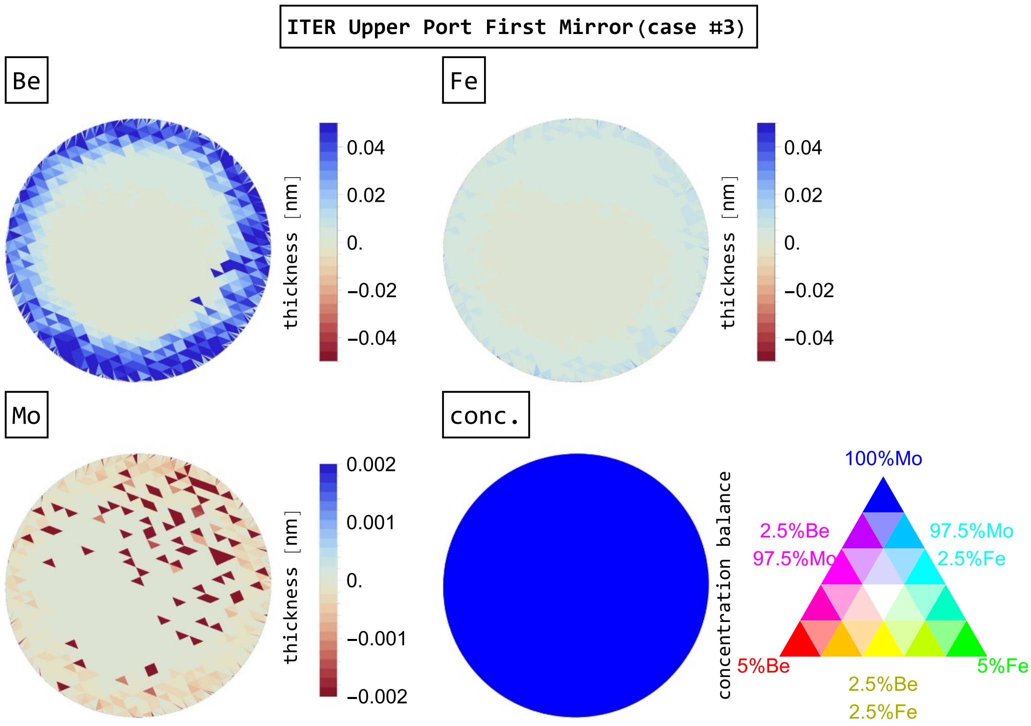

Figure 12. Net fluences of Be (top left), Fe (top right) and Mo (bottom left) on the upper port first mirror front surface at the end of the simulation—net erosion is shown in red, net deposition in blue. Bottom right picture shows surface composition in a 100 nm surface layer.

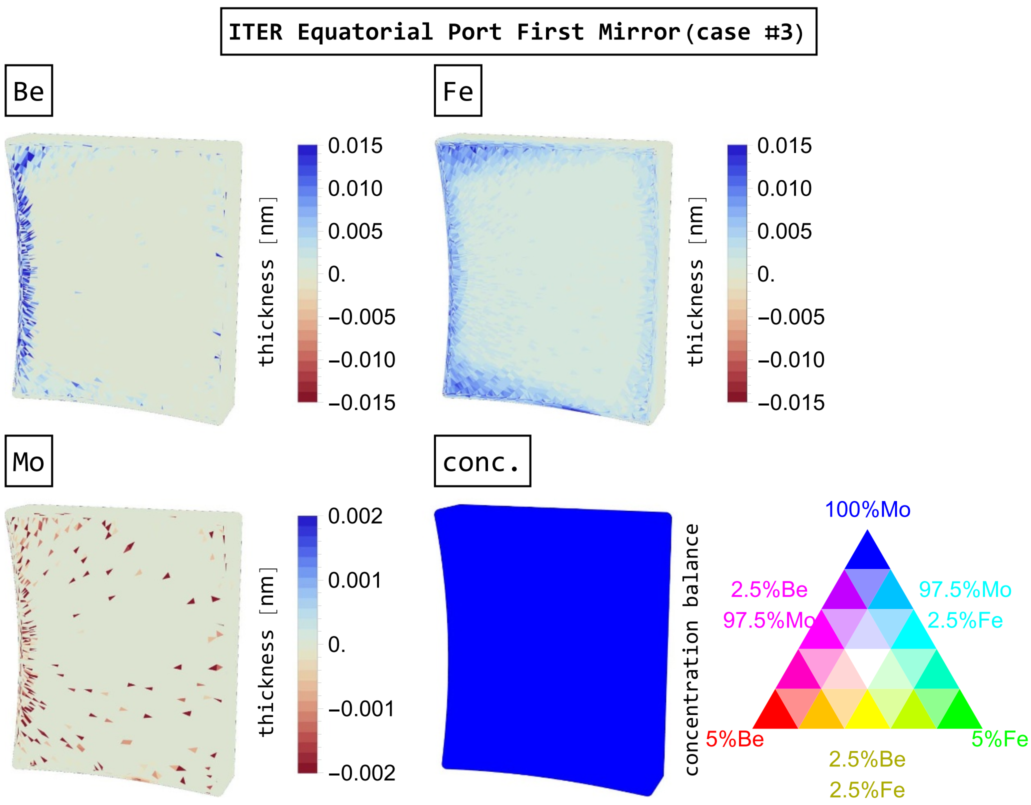

Figure 13. Net fluences of Be (top left), Fe (top right) and Mo (bottom left) on the equatorial port first mirror front surface at the end of the simulation—net erosion is shown in red, net deposition in blue. Bottom right picture shows surface composition in a 100 nm surface layer.

Table 6. Second mirrors: overview of average Mo, Be and Fe deposition on the front of the mirror surfaces at the end of the simulation time—fluxes simulated by ERO2.0 were integrated over time and mirror front surface, and converted to a layer thickness using the element's density.

		Mo layer (nm)	Be layer (nm)	Fe layer (nm)
case #1	Upper	0.03	0.24	0.35
	Equatorial	0.14	0.03	0.15
case #2	Upper	5.63×10^{-3}	0.07	0.04
	Equatorial	0.01	3.81×10^{-3}	0.02
case #3	Upper	6.86×10^{-5}	8.09×10^{-4}	5.47×10^{-4}
	Equatorial	1.26×10^{-4}	4.65×10^{-5}	1.73×10^{-4}

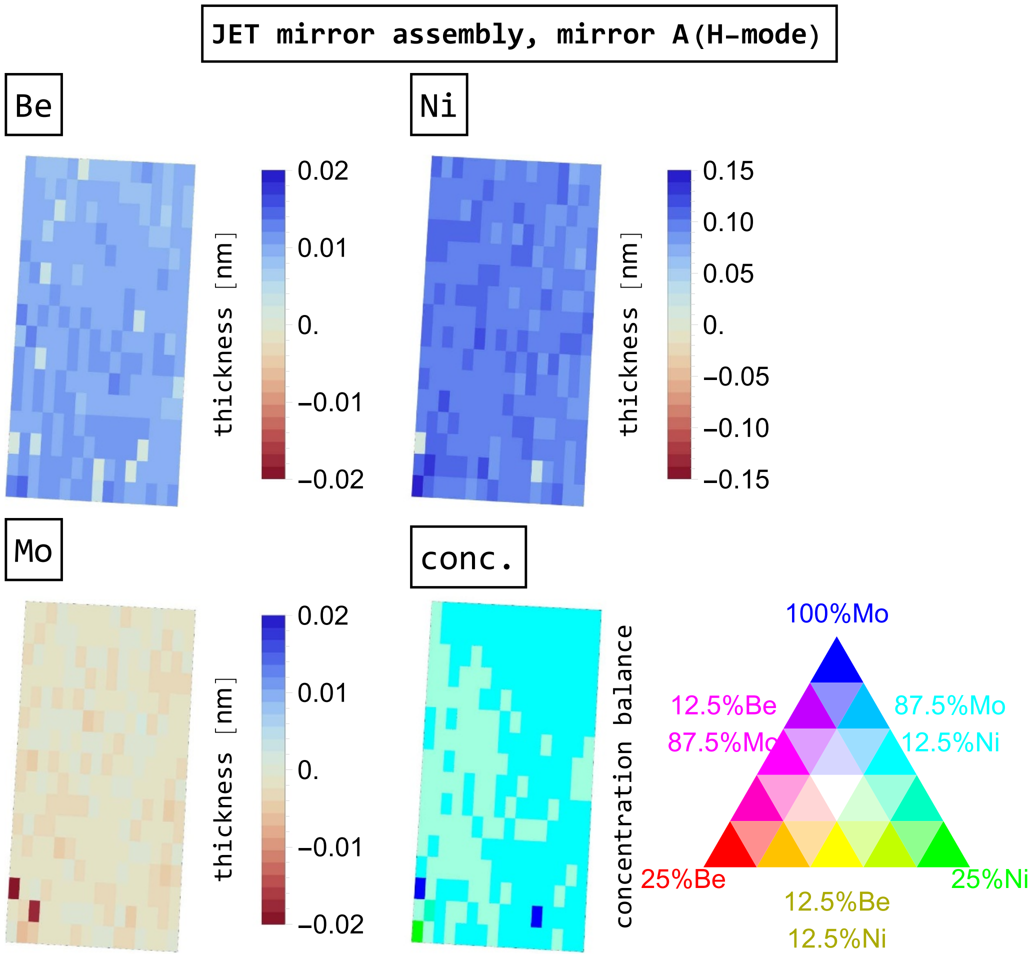

Figure 14. Net fluences of Be (top left), Ni (top right) and Mo (bottom left) on JET mirror A in the H-mode case—net erosion is shown in red, net deposition in blue. Bottom right picture shows surface composition in a 1 nm surface layer—the mean surface composition is 1.7% Be, 12.9% Ni and 85.4% Mo.

exclusively particles coming in a straight line from the plasma hit the mirror. All in all, the sputtering is caused by more than 99% by D.

In the experimental campaign described and analysed in detail in [8], the mirrors were exposed to 8 h of H-mode discharges and 15.3 h of L-mode discharges. The net fluences of the two separate H-mode and L-mode simulations were added up to make a direct comparison with the experiment possible.

The following caveats however should be noted: the simulations in the two plasma cases were conducted separately and not in succession, so both times the mirror started with a pure Mo surface; as mentioned before, mirror holder geometries were used (in the experiment, each holder holds two mirrors for a total of six mirrors), but since atomic surface concentrations are compared, and since the holders are parallel to the mirror surfaces, this should not lead to significant differences;

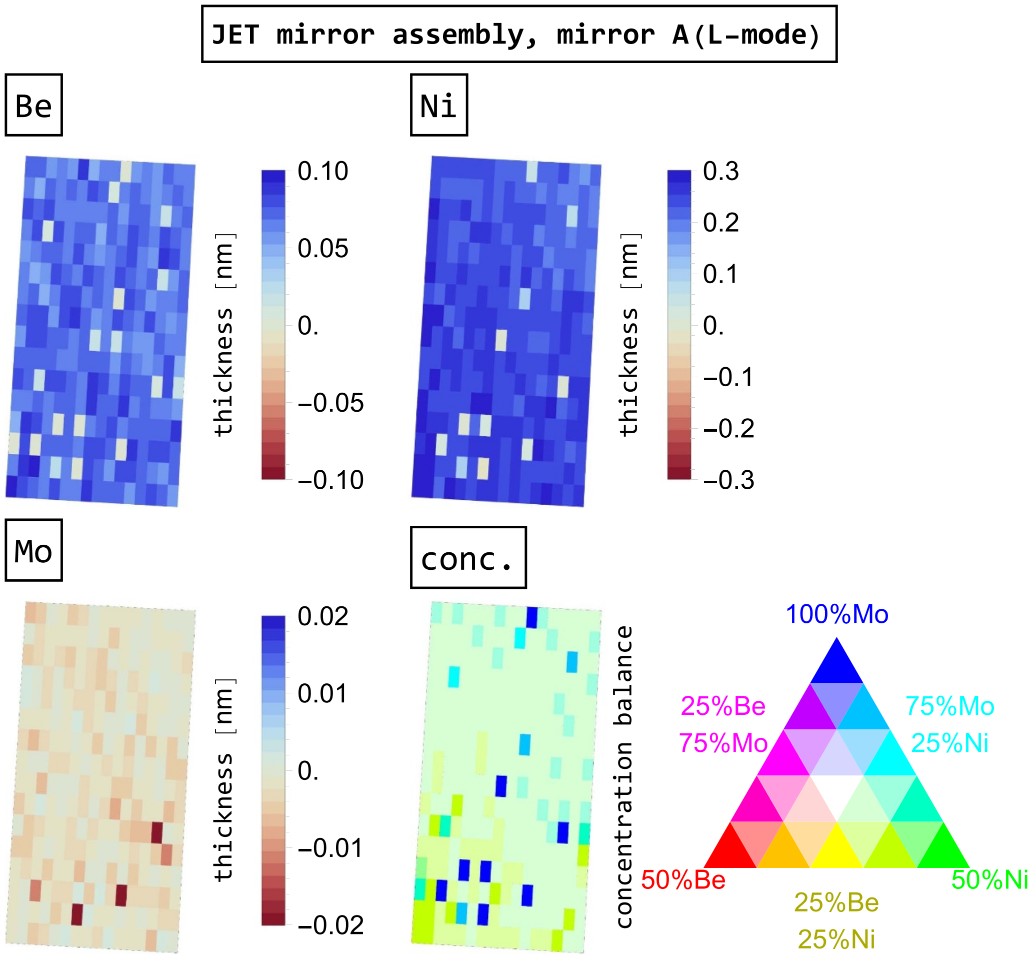

Figure 15. Net fluences of Be (top left), Ni (top right) and Mo (bottom left) on JET mirror A in the L-mode case—net erosion is shown in red, net deposition in blue. Bottom right picture shows surface composition in a 1 nm surface layer—the mean surface composition is 10.1% Be, 26.8% Ni and 63.1% Mo.

Table 7. Comparison of accumulated surface density of beryllium and sputtered wall material between simulation (this work) and experiment [8]. Notes: experimental detection limit: $\sim 0.5 \cdot 10^{15}$ cm^{-2}; two mirrors in each location in experiment, one mirror holder surface in simulation; experimental values shown as Ni are combined values for all materials sputtered from the assembly (Ni+Cr+Fe); simulation values are added up from two separate simulations for the H- and L-mode phases with exposure times according to experiment (comp. table 2).

	Be deposition (10^{15} cm^{-2})			Ni deposition (10^{15} cm^{-2})		
Mirror	Simulation	Experiment		Simulation	Experiment	
A	0.96	<0.5	<0.5	3.11	2.5	3.0
B	0.86	<0.5	4.8	3.39	2.2	3.7
C	0.25	<0.5	3.9	12.42	1.5	1.6

and finally, the plasma backgrounds are assumed as constant, while the experimental results are campaign-averaged over the exposure time.

In the experimental analysis, many elements were found on the mirrors, with the highest measured concentrations being C and O, with smaller amounts of Be, N and metallic materials (Ni, Cr, Fe). In the presented ERO2.0 simulations, no C, O, Fe or Cr were considered, with the metal components being approximated by pure Ni. In [8], different possible sources for C and O were discussed, e.g. post-exposure oxidisation before the analysis for O and trace sources of diamond dust from polishing processes for C. Because these processes are not related to the actual exposure of the mirrors inside JET, they were not included in the simulation and thus, the comparison here focusses on the Be and Ni data. Be densities of 4–5$\cdot 10^{15}$ cm^{-2} were measured on two mirrors located on holders B and C, with no Be found in position A. The simulated values of 0.12$\cdot 10^{15}$ cm^{-2} lie slightly below the detection limit mentioned in the reference ($\sim 0.5 \cdot 10^{15}$ cm^{-2}), which falls in line with the fact that on four of the six mirrors in the experiment, no Be was detected at all. The combined values roughly agree with the experimental values where deposition was found, although experimentally the highest Be deposition was found on mirror C where the simulation predicts the lowest value. For Ni, the experimental analysis showed deposition on all mirrors, in the range of 1.5–3.7$\cdot 10^{15}$ cm^{-2}. These results match the simulated results of 3.11–3.39$\cdot 10^{15}$ cm^{-2} quite well for mirrors A and B, with the caveat that [8] lists values for Ni, Cr and Fe combined. Mirror C simulation results differ significantly in the Ni deposition values compared to the experiment. This can likely be attributed to the fact that the deuterium fluxes (responsible for the largest fraction of Ni sputtering) coming into entrance C of the assembly were likely overestimated, as the total flux into the assembly simulated by EIRENE was spread over the surfaces of the first set of catcher planes covering the cone entrances. Entrance C does not have a cone structure, but only a hole in the assembly and lies further out than the two cone entries (see figure 3). The total flux was only scaled by the area of the entrance, but a more refined approach would also take into account the distance to the plasma, which is different only for entrance C. Thus, mirrors A and B are assumed to have more realistic simulation results than mirror C.

4. Conclusions and outlook

In this paper, ERO2.0 simulations with input from EIRENE, SOLPS-4.3, EDGE2D-EIRENE and SDTrimSP were presented. With this three-stage multi-code simulation setup, meaningful results for erosion and deposition on diagnostic FMs in recessed areas of JET and ITER were achieved. Results in the JET ITER-like mirror assembly were in good agreement with an experimental analysis, showing the validity of the approach for novel recessed area simulations based on ERO2.0. For ITER, predictions for FMs in two diagnostic ports were presented and we conclude that over the whole expected ITER pre-fusion and fusion power operation time, the deposition and erosion on the mirrors are likely negligible—in the worst case from our analysis (case #1, upper port), barely 1 nm of impurities is deposited in the central part of the mirror. Importantly, the geometry of the DFW in front of the FM is likely to have a significant impact on the transport of particles in the recessed volume, which can be seen from the strong local pattern of deposition in all the simulated plasma cases. We expect that with slight adjustments to the cone structure in front of the mirror, even the fluxes onto the edge region of the mirror could be avoided and thus, the total erosion and deposition of the mirror front surface be further reduced. Our simulations showed that with the provided DFW geometry, the centre of each mirror is subjected to only minimal fluxes compared to the edge, so we expect that cleaning of the mirrors is likely not needed under the given assumptions. Detailed information about reflection properties is, however, outside of the scope of the present studies.

Some uncertainties remain in the approach: most significantly, the plasma solutions from validated plasma codes had to be extrapolated to generate a plasma background for the local ERO2.0 simulations. In some geometries, the extrapolation distance was up to 18 cm, which comes with a large uncertainty. While obtaining plasma solutions in the complex 3D geometry inside the DFW in ITER is not possible with the current modelling tools, the availability of wide-grid solutions covering the volume up to first wall elements steadily increases and such a plasma background would reduce the extrapolation gap to the recessed volumes analysed in this work significantly and thus improve the quality of the results.

Concerning the plasma backgrounds, steady-state operation was assumed throughout the simulations, in which the fluxes into recessed areas are very low. Processes that deposit more material even in recessed areas could lead to significantly more deposition on the FMs. In particular, boronisation as a wall conditioning measure is likely to deposit layers of boron even on the DFW during the boronisation process, and while the FMs could be kept clean with the help of shutters during boronisation, the deposited layers on the cone in front of the mirror are likely to erode over time and release potentially significant amounts of material close to the mirror. The three-stage approach presented in this work should be easily adjustable to include this mechanism and thus provide important results for operation of the FMs in a regularly boronised device.

Finally, as the computing power of high-performance computers increases, ERO2.0 simulations with even more test particles will also be viable and would increase the resolution of the results, as even with the massive amount of test particles that were used in the presented simulations, rare high-energy CXN particles are still not resolved perfectly, as can be seen in the spikes of erosion in certain isolated locations in all presented ITER FM cases.

Acknowledgments

This work has been carried out within the framework of the EUROfusion Consortium, funded by the European Union via the Euratom Research and Training Programme (Grant Agreement No 101052200—EUROfusion). Views and opinions expressed are those of the author(s) and do not necessarily reflect those of the European Union, the European Commission or the ITER Organization. Neither the European Union nor the European Commission can be held responsible for them. The authors gratefully acknowledge the computing time granted by the JARA Vergabegremium and provided on the JARA Partition part of the supercomputer JURECA [14] at Forschungszentrum Jülich. This work benefitted from HPC resources from CINECA Marconi-Fusion project FUA36 WPJET1. This work has been carried out within the framework of an ITER service Contract IO/20/CT/4300002242.

ORCID iDs

S. Rode https://orcid.org/0009-0009-7614-5218
S. Brezinsek https://orcid.org/0000-0002-7213-3326
M. Groth https://orcid.org/0000-0001-7397-1586
A. Kirschner https://orcid.org/0000-0002-3213-3225
D. Matveev https://orcid.org/0000-0001-6129-8427

R.A. Pitts https://orcid.org/0000-0001-9455-2698
J. Romazanov https://orcid.org/0000-0001-9439-786X
A. Terra https://orcid.org/0000-0003-0638-6103
T. Wauters https://orcid.org/0000-0002-2941-7817
S. Wiesen https://orcid.org/0000-0002-3696-5475

References

[1] Kotov V. 2016 *Nucl. Fusion* **56** 106027
[2] Romazanov J. *et al* 2020 *Contrib. Plasma Phys.* **60** e201900149
[3] Rode S. , Brezinsek S., Kirschner A., Moser L., Pitts R., Romazanov J., Terra A., Wauters T. and Wiesen S. 2024 *Nucl. Mater. Energy* **38** 101564
[4] Kukushkin A.S. *et al* 2011 *Fusion Eng. Des.* **86** 2865–73
[5] Lisgo S.V., Kukushkin A., Pitts R.A. and Reiter D. 2013 *J. Nucl. Mater.* **438** S580–4
[6] Reiter D. , Baelmans M. and Börner P. 2005 *Fusion Sci. Technol.* **47** 172–86
[7] Mutzke A. *et al* 2019 SDTrimSP version 6.00 Report IPP 2019- 02 *Technical Report* Max-Planck-Institut für Plasmaphysik
[8] Rubel M. , Moon S., Petersson P., Widdowson A., Pitts R.A., Aleiferis S., Fortuna-Zaleśna E., De Temmerman G. and Reichle R. 2021 *Nucl. Fusion* **61** 046022
[9] Romazanov J. *et al* 2021 *Nucl. Mater. Energy* **26** 100904
[10] Romazanov J. *et al* 2022 *Nucl. Fusion* **62** 036011
[11] Romazanov J. *et al* 2019 *Nucl. Mater. Energy* **18** 331–8
[12] Groth M. *et al* 2013 *Nucl. Fusion* **53** 093016
[13] Pitts R.A. *et al* 2019 *Nucl. Mater. Energy* **20** 100696
[14] Jülich Supercomputing Centre 2021 *JLSRF* **7** A182